Published in Journal of Modern Optics 40, issue 4, 637 - 645, 1993
which should be used for any reference to this work

Beam shaping of high-power laser diode arrays by continuous surface-relief elements

P. EHBETS†, H. P. HERZIG†, R. DÄNDLIKER†,
P. REGNAULT‡ and I. KJELBERG‡

† Institute of Microtechnology, University of Neuchâtel,
Rue A.-L. Breguet 2, CH-2000 Neuchâtel, Switzerland
‡ Centre Suisse d'Electronique et de Microtechnique S.A. (CSEM),
Maladière 41, CH-2007 Neuchâtel, Switzerland

Abstract. A breadboard for beam shaping of high-power laser diode arrays (LDAs) has been realized. The coherent beams are added with the aid of a continuous surface-relief fan-in element. It results in a nearly symmetric single lobed beam of collimated light with maximum conversion efficiency. The theoretical efficiency is determined to be 96·7%. Experimentally, one third of the total power is now in the central peak.

1. Introduction

Semiconductor lasers are used in optics as compact, monochromatic light sources, that can be directly modulated. Some applications, such as communication between satellites and pumping of fibre lasers, require high power and near fundamental mode beam quality. High power can be achieved by phase-locked laser diode arrays (LDAs). Unfortunately, LDAs generate poor quality output beams, which cannot be collimated properly by conventional diode laser optics. In this paper we demonstrate the conversion of a multi-lobed near-field emitted by ten stripes of a LDA into a single-lobed Gaussian beam of collimated light.

The lateral modes of laser diode arrays are defined by the periodic gain and refractive index distribution across their widths. These modes can be described by coupled-wave theory [1]. The 180° out-of-phase mode seems to be the most stable mode in parallel filament arrays. Consequently, these lasers show a double lobed far-field. In order to improve the optical quality of the LDA output, different possibilities have been proposed. Using a phase plate, the 180° mode can be converted in a 0° mode [2], which leads to a relatively strong central lobe with smaller side lobes, as shown in figure 1. For one-dimensional arrays the light distribution is highly asymmetric. This is inadequate to fill the aperture of a collimator uniformly. The side lobes can be eliminated by an additional afocal system [3]. The system uses a d.c. phase shifter in the back focal plane of the first lens and a binary phase corrector element in the back focal plane of the second lens. However, the asymmetry of the light distribution is not removed. Another method uses a lens and a binary fan-in grating to superimpose N lasing apertures, converting the laser array into a single emitter with about N times the power density [4]. In this case the shape of the beam is determined by the aperture of a single laser stripe (figure 1). The coherent addition is only efficient when the beams are in the correct phase state. This has been achieved by an external cavity including the laser array and also the binary fan-in grating.

Higher efficiency close to 100% can be achieved by coherently adding N lasers with the aid of continuous surface-relief gratings [5]. Our approach is based on the

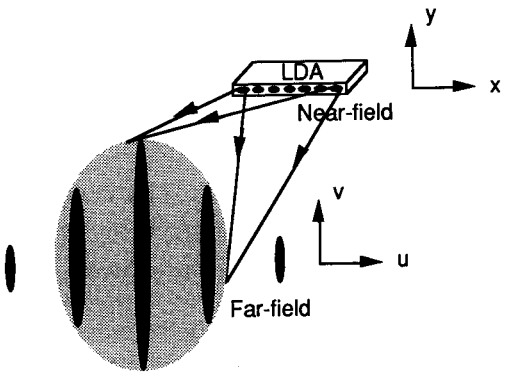

Figure 1. Far-field pattern of coupled laser diode array: the black pattern corresponds to the 0° mode; the grey pattern is the far-field of a single stripe.

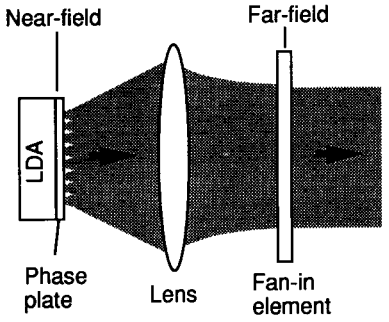

Figure 2. Basic arrangement for far-field shaping.

tandem component shown in figure 2. A phase-locked LDA is chosen that emits only one transversal mode. The LDA, that was used for the experiment, fulfilled this condition only near threshold. For higher driving currents, several lateral modes of the LDA started to lase. For this reason, an external cavity should be used for high power, in order to increase the modal separation and enhance the coherence. Other array structures, like Y-guides [6] or resonant-optical waveguides [7], provide much better spatial-mode selectivity and stability. Therefore, even at high power no external cavity is needed for an efficient beam shaping. The optimum phases are now introduced by a phase plate at the LDA output. The fan-in element has a continuous surface-relief profile enabling maximum conversion efficiency. A compact bread-board for beam shaping of high power LDAs has been realized. We summarize briefly the theory and then we present our experimental results.

2. Theory

The basic concept for the far-field shaping is shown in figure 2, where N beams emitted by a LDA are added coherently. The fan-in element is only efficient for a well defined phase relationship between the emitted beams. If the LDA operates in a stable single mode, these phases can be established with a phase plate in the near-field. In the following, we calculate the optimum phases and the corresponding fan-in element for an efficient beam shaping.

In our model, the near-field distribution $U(x, y)$ at the LDA output, after the phase plate, is approximated by an array of N Gaussian beams. We restrict the analysis to the case of one-dimensional arrays, but the same principle can be applied for two-dimensional arrays. Under these assumptions the near-field of the LDA can be written as

$$U(x,y)=\sum_{m=1}^{N} A_m \exp(\mathrm{i}\phi m)\exp\left[-\frac{(x-x_m)^2}{w_x^2}-\frac{y^2}{w_y^2}\right], \tag{1}$$

where A_m is the amplitude, ϕ_m the phase, and x_m the position of the mth Gaussian beam. We assume a constant spacing between two neighbouring beams, defined by $s=x_{m+1}-x_m$. For index-guided LDAs, the number of Gaussian beams in the near-field corresponds to the number of array elements and their beam waist radii w_x and w_y are mainly determined by the geometry of a single stripe [8]. Whereas, gain-guided LDAs can produce lateral modes with more lobes in the near-field than waveguides [9]. In such a situation, the number of Gaussian beams has to be increased, in order to describe the near-field distribution accurately.

The far-field distribution $\hat{U}(u, v)$ is related to the near-field $U(x, y)$ by a Fourier transform. Thus, we get for the far-field

$$\begin{aligned}\hat{U}(u,v)&=\int_{-\infty}^{\infty} U(x,y)\exp[2\pi\mathrm{i}(xu+yv)]\,\mathrm{d}x\,\mathrm{d}y\\&=c_1\exp[-\pi^2(w_x^2u^2+w_y^2v^2)]\sum A_m\exp(\mathrm{i}\phi_m)\exp(2\pi\mathrm{i}x_mu),\end{aligned} \tag{2}$$

or expressed in amplitude and phase

$$\hat{U}(u,v)=|\hat{U}(u,v)|\exp[\mathrm{i}\Psi(u,v)], \tag{3}$$

where $\Psi(u,v)=\arg\{\hat{U}\}$ and c_1 is a constant.

As the emission of every array element interferes with each other, interference patterns in the far-field intensity distribution with periodicities of $1/s$, $1/2s, \ldots,$ $1/(N-1)s$ can be observed. If the interference terms of equal spatial frequency are collected, the intensity distribution in the grating plane can be written as

$$\begin{aligned}I(u,v)=|\hat{U}|^2&=c_2\exp[-2\pi^2(w_x^2u^2+w_y^2v^2)]\\&\times\left[\sum_{m=1}^{N}A_m^2+2\sum_{p=1}^{N-1}B_p\cos(2\pi psu+\Phi_p)\right].\end{aligned} \tag{4}$$

For a given set A_i, ϕ_i, the coefficients B_p, Φ_p for one spatial frequency component of the interference pattern can be calculated from the equations

$$B_p^2=\left[\sum_{m=1}^{N-p}A_mA_{m+p}\cos(\phi_m-\phi_{m+p})\right]^2+\left[\sum_{m=1}^{N-p}A_mA_{m+p}\sin(\phi_m-\phi_{m+p})\right]^2, \tag{5}$$

$$\Phi_p=\arctan\left(\frac{\sum_{m=1}^{N-p}A_mA_{m+p}\sin(\phi_m-\phi_{m+p})}{\sum_{m=1}^{N-p}A_mA_{m+p}\cos(\phi_m-\phi_{m+p})}\right). \tag{6}$$

The envelope of the intensity distribution $I(u, v)$ determined by equation (4) is the desired Gaussian far-field distribution, corresponding to the far-field of a single stripe. If we are able to eliminate the variations in the interference patttern, the intensity distribution becomes equal to that Gaussian envelope. According to

equation (3), the remaining phase distribution could then be converted into a plane wave by a phase element with transmittance equal to $\exp[-i\Psi(u,v)]$. An interference term close to a constant value can be achieved by requiring minimum variance, namely

$$\int_{-\infty}^{\infty}\int_{-\infty}^{\infty}\left[\sum_k B_k \cos(2\pi ksu+\Phi_k)\right]^2 du\,dv\rightarrow\min. \tag{7}$$

Since the terms of different spatial frequency are orthogonal, the minimum condition becomes finally

$$\sum_k B_k^2\rightarrow\min. \tag{8}$$

The minimization of equation (8) yields the optimized phases ϕ_m for a given set of amplitudes A_m.

We summarize the beam shaping process sketched in figure 2. A set of amplitudes A_m and phases ϕ'_m is known at the LDA output. The optimum set of phases ϕ_m can be found by minimization of equation (8). The phase differences between the optimum phases ϕ_m and the phases ϕ'_m of the LDA have to be added by a phase plate. The optimized intensity distribution $I(u,v)$ in the far-field is then given by equation (4) and the phase distribution $\Psi(u,v)$ by equations (2) and (3). In order to generate a plane wave a second phase element has to be added to compensate $\Psi(u,v)$ in the far-field. Its complex amplitude transmittance is

$$T(u,v)=\exp[-i\Psi(u,v)]. \tag{9}$$

The optimization of equation (8) is a numerical problem, which has been solved by using the Downhill Simplex Method [10].

3. Experimental results

Figure 3 shows the breadboard for far-field shaping of LDA mounted on a large heatsink. The continuous surface-relief fan-in element can be observed in front of the assembled prototype. The system includes a LDA, a phase plate, a lens, and a fan-in element as already depicted in figure 2.

For our experiments, we have used a SDL-2420 LDA from Spectra Diode Labs, which is a gain-guided device and offers ten phase coupled emitters spaced by 10 μm, operating at the wavelength $\lambda = 801$ nm. Spectral analysis of the near-field has shown that near threshold, the LDA operates in a single lateral mode, which is known as the $\nu = 10$ mode [8]. For this mode the emitters possess an alternating 0/180° phase state producing the double lobed far-field shown in figure 4.

The phase plate that should generate the optimized phases consists of 10 zones each of 10 μm width. The element is fabricated at CSEM by reactive ion etching (RIE) into fused silica. Repeated etching produces discrete levels. We have distributed the 10 optimum phases on 16 equally spaced levels between 0 and 2π. It results that in this special case the etch with depth corresponding to a phase delay of $\pi/4$ is not necessary and therefore, three etching steps were sufficient to generate the required levels.

The optimized phases ϕ_i are shown in the first row of the table. In the second row the quantized values for the phase plate are listed. Illuminated with the $\nu = 10$ mode the phase plate generates the optimized phases. The quantization error is within $\pm\lambda/40$. Theoretically 97·3% of the power emitted by the LDA can be collimated into

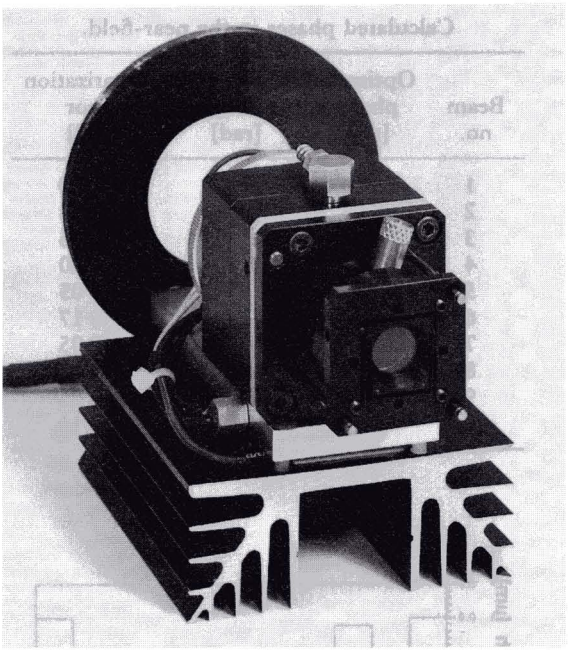

Figure 3. Breadboard of LDA shaping mounted on a heat-sink.

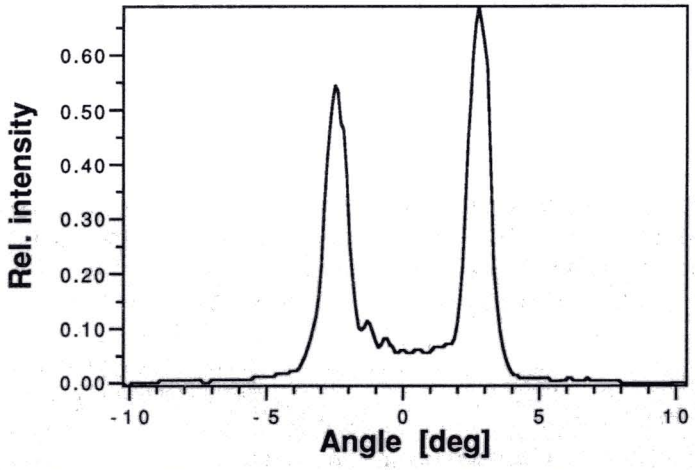

Figure 4. Measured double lobed far-field of 180° mode.

a single Gaussian beam. Due to the quantization of the optimized phases the efficiency drops slightly to 96·7%. Figure 5 shows the calculated profile of the phase plate. In comparison, figure 6 shows a scanning electron microscope (SEM) picture of the fabricated phase plate. The accuracy of the depth profile is better than 1%.

A lens with short focal length of $f = 14{\cdot}5$ mm has been chosen to get a compact system. This defines the periodicity of the fan-in element in the Fourier plane of the lens (figure 2) to be $p = \lambda f / s = 1{\cdot}16$ mm. The number of periods illuminated in the far-field is inversely proportional to the fill-factor of the LDA, which is defined by

Calculated phases in the near-field.

Beam no.	Optimum phases [rad]	Quantized phase plate [rad]	Quantization error [rad]
1	0·00	0·00	0·00
2	0·52	3·53	−0·13
3	0·24	0·39	0·16
4	5·11	1·96	0·00
5	5·05	5·11	0·05
6	1·41	4·71	0·17
7	1·52	1·57	0·05
8	4·58	1·57	0·13
9	2·02	1·96	−0·06
10	4·61	1·57	0·10

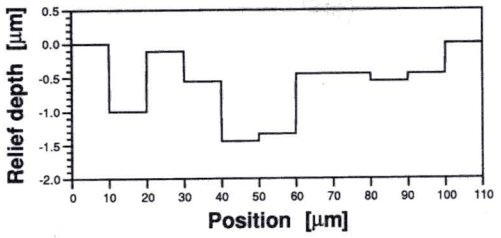

Figure 5. Calculated profile of the phase plate.

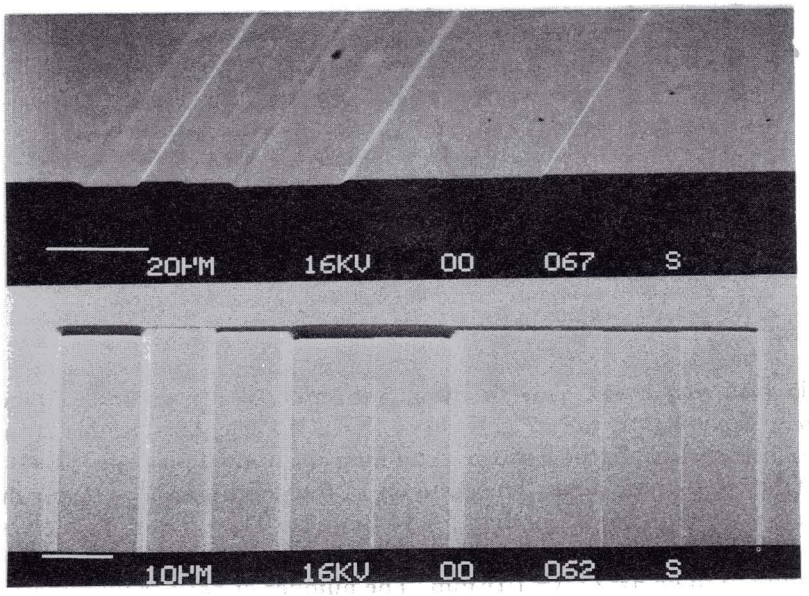

Figure 6. SEM pictures of the fabricated phase plate: side view, top view.

the ratio of the Gaussian beam diameter and the stripe spacing. In our case, about three periods of the fan-in element were illuminated.

According to equation (9) the fan-in element has to generate a phase distribution of $-\Psi(u, v)$ in the far-field. This is achieved by a continuous surface-relief element in the back focal plane of the lens (figure 2). The thickness modulation is obtained from the phase distribution by the following relation

$$d(x, y) = d_0 + \Psi(x = \lambda f u, y = \lambda f v) \frac{\lambda}{2\pi(n-1)}, \tag{10}$$

where d_0 is a constant thickness and $(n-1)$ is the refractive index difference between medium and air. In our experiment, we have calculated the far-field from equations (2) and (3) for constant amplitudes A_m and for the quantized optimized phases ϕ_m. The resulting thickness variation is the continuous function shown in figure 7 (*a*). It is known that for even numbered arrays the profile of fan-in elements has phase steps of π (e.g. [11]). In order to avoid discontinuity in the profile we have translated our LDA by half a period, i.e. by $s/2$ with respect to the fan-in element. This is equivalent to an additional wedge in the Fourier plane, which slightly deflects the outgoing beam.

The element is written in photoresist using the laser-beam writing system at the Paul Scherrer Institute, Zurich [12]. The photoresist is exposed with a scanning laser beam of controllable intensity and then etched by a developer. The fidelity of

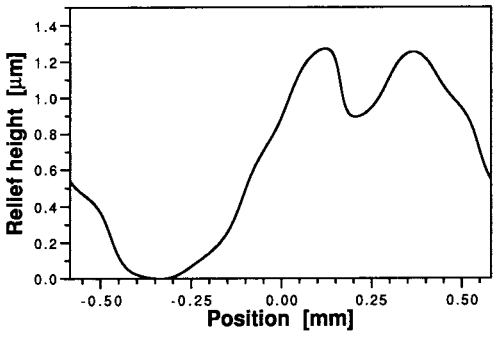

(*a*)

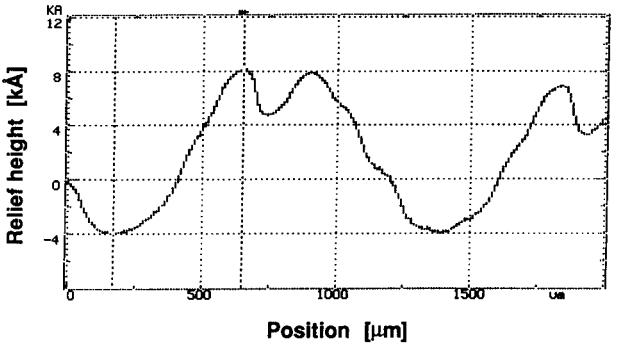

(*b*)

Figure 7. Profile of the fan-in element: (*a*) theory, (*b*) measured.

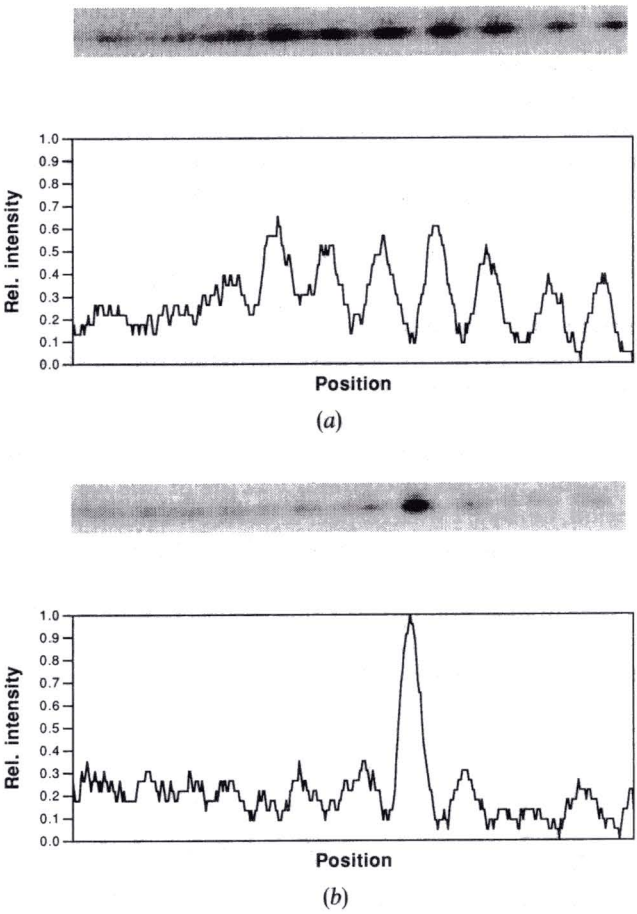

Figure 8. Source array (*a*) before shaping and (*b*) after shaping. It results in a nearly symmetric single lobed beam.

the resulting relief profile relies on the knowledge and reproducibility of the photoresist response. Finally, the phase element is baked and measured with a stylus profilometer. One typical measured profile is shown in figure 7 (*b*).

In the case of perfect shaping one collimated beam should come out of the shaping system (figure 2). We have focused this beam on to a CCD camera, where we can observe the virtual source. Figure 8 (*a*) shows the source array before shaping. In this case, we have removed the fan-in grating. Then the ten array elements can be identified. Unfortunately, the LDA does not emit a nice symmetric near-field. The first three lobes are hardly detectable. This asymmetry might be due to the effects of non-uniform heat sinking, non-uniform gain across the array, or unwanted back reflection from the phase plate, which was not antireflective coated. Figure 8 (*b*) shows the virtual source after adding the fan-in element. It results in a single bright spot as predicted by theory with nearly symmetric aspect. One third of the total power is now in the central peak.

The poor performance cannot be explained by the quality of the shaping elements. The phase plate and the fan-in element are sufficiently accurate. The fact

that the amplitude distribution of the source array was not uniform, as assumed for the design of the element, seems not to be important, either. Numerical simulations show that the efficiency should only drop down to 96·0% for the observed near-field amplitude distribution (figure 8(*a*)) and to 87·5% for the theoretical half-sinus amplitude modulation of the $v=10$ mode. The efficiency of the shaping depends much more on the relative phases of the emitters. For this reason, it is assumed that the phase plate was placed at a position where the different beams did already partially overlap. For future use, antireflection coatings on the elements are recommended to avoid feedback into the LDA.

4. Conclusions

We have shown that stable eigenmodes emitted by LDAs can be shaped and collimated with very small inherent losses. The proposed method produces a nearly symmetric single lobed beam of collimated light with maximum conversion efficiency. A compact breadboard has been built for shaping an array of ten elements. The system includes a multilevel phase plate at the LDA output to produce in the far-field a smooth intensity distribution, which corresponds to the far-field of a single stripe of the laser array. The structure of the array is converted into a phase distribution in the far-field. This phase distribution is then corrected by a continuous surface-relief fan-in grating. The theoretical efficiency for this set-up is 96·7%. Experimentally, we have found one third of the total power in the central peak.

References

[1] MEHUYS, D., and YARIV, A., 1988, *Optics Lett.*, **13,** 571.

[2] HEIDEL, J. R., RICE, R. R., and APPELMAN, H. R., 1986, *Quant. Electron. Lett.*, **22,** 749.

[3] LEGER, J. R., SWANSON, G. J., and HOLZ, M., 1987, *Appl. Phys. Lett.*, **50,** 1044.

[4] LEGER, J. R., SWANSON, G. J., and VELDKAMP, W. B., 1987, *Appl. Optics*, **26,** 4391.

[5] HERZIG, H. P., DÄNDLIKER, R., and TEIJIDO, J. M., 1989, *Holographic Systems, Components and Applications*, Bath, UK, Conference Publication No. 311 (London: Institution of Electrical Engineers), pp. 133–137.

[6] WELCH, D. F., CROSS, P., SCIFRES, D., STREIFER, W., and BURNHAM, R. D., 1986, *Electron. Lett.*, **22,** 293.

[7] MAWST, L. J., BOTEZ, D., JANSEN, M., ROTH, T. J., TU, C., and ZMUDZINSKI, C., 1991, *Electron. Lett.*, **27,** 1586.

[8] BOTEZ, D., 1988, *IEEE J. quant. Electron.*, **24,** 2034.

[9] HADLEY, G. R., HOHIMER, J. P., and OWYOUNG, A., 1986, *Appl. Phys. Lett.*, **49,** 684.

[10] PRESS, W. H., FLANNERY, B. P., TEUKOLSKY, S. A., and VETTERLING, W. T., 1989, *Numerical recipes in Pascal* (Cambridge University Press).

[11] MORRISON, R. L., 1992, *J. opt. Soc. Am.* A, **9,** 464.

[12] GALE, M. T., LANG, G. K., RAYNOR, J. M., SCHÜTZ, H., and PRONGUÉ, 1992, *Appl. Optics*, **31,** 5712.